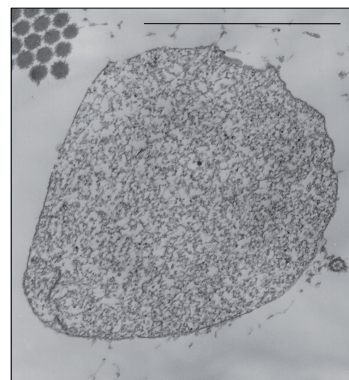
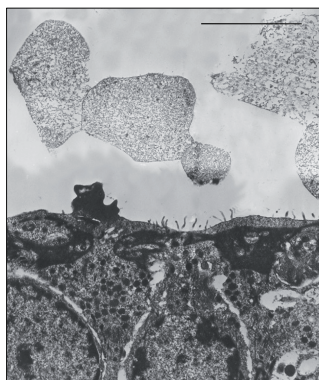
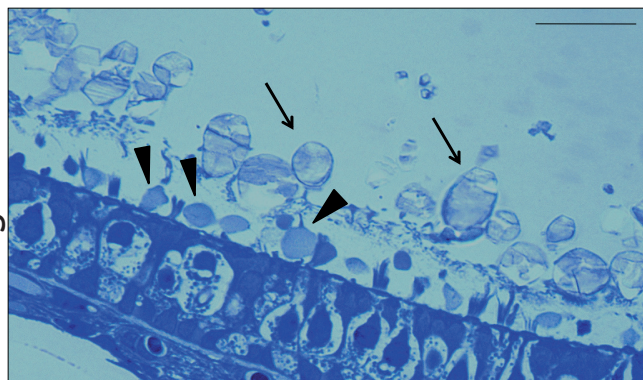
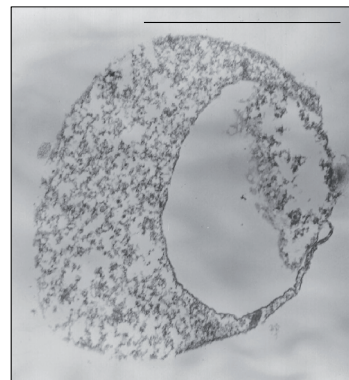
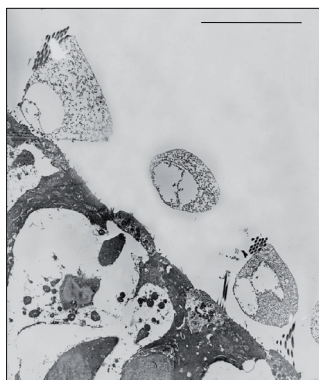
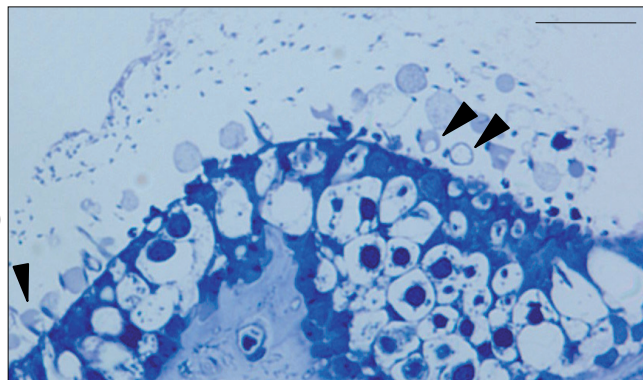
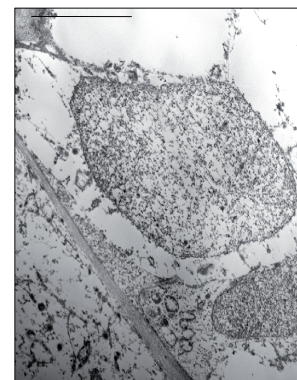
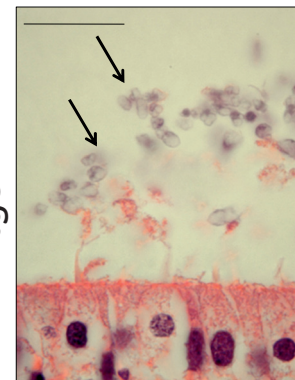
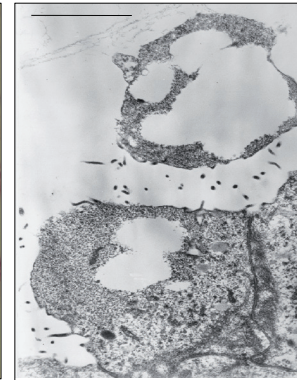
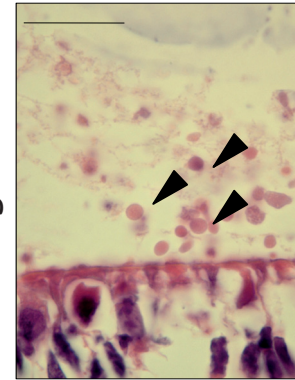
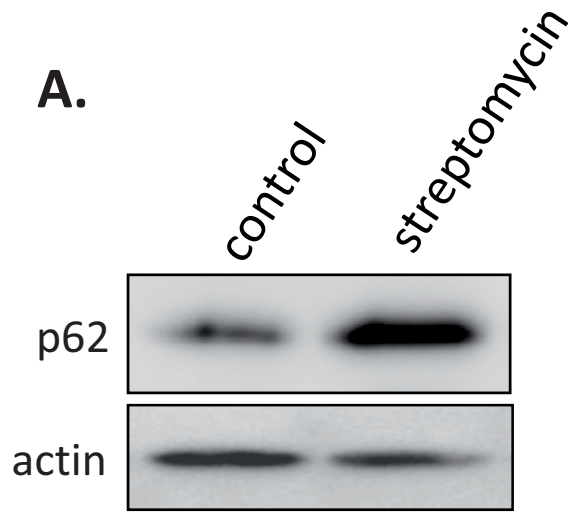
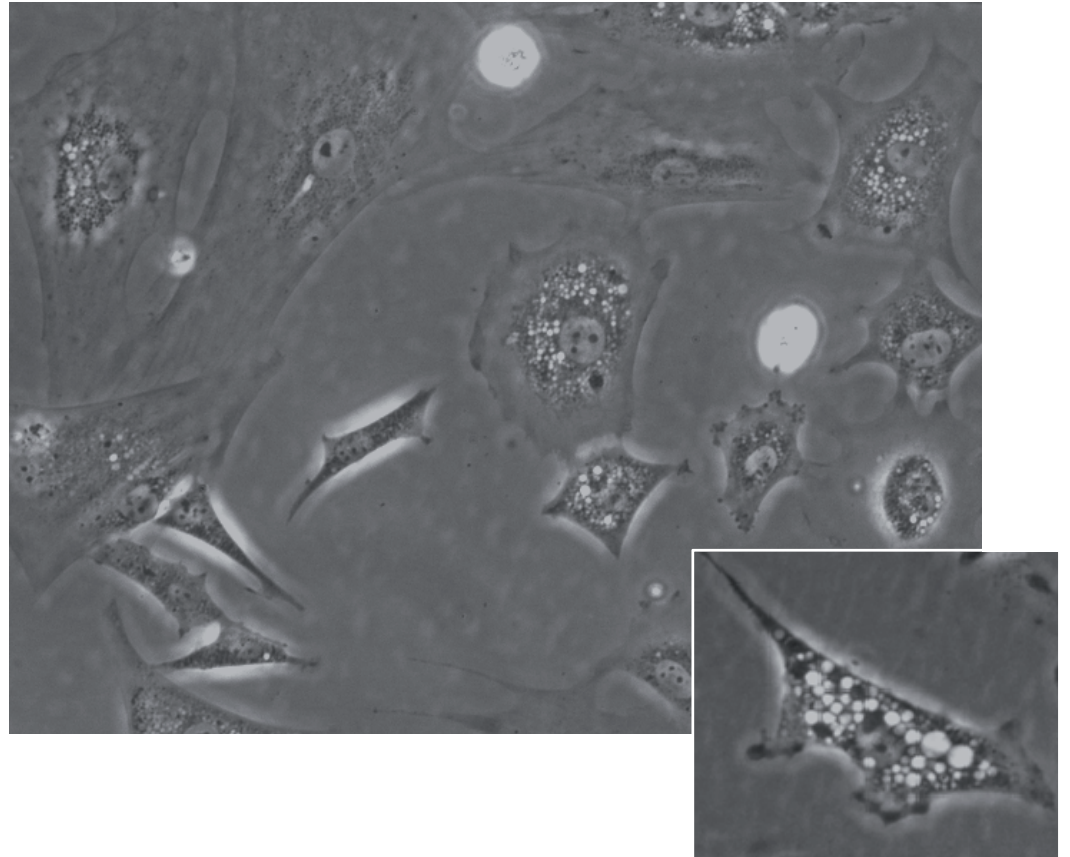


A.*Atg4B*^{+/+}*Atg4B*^{-/-}**B.***Atg5*^{+/+}*Atg5*^{-/-}



B.

Streptomycin 1 mg/ml for 6 days



Marino et al. Figure.S5

[Map Viewer Home](#)

[Map Viewer Help](#)
[Mouse Maps Help](#)
[FTP](#)

[Data As Table View](#)

[Maps & Options](#)

[Compress Map](#)

Region Shown:

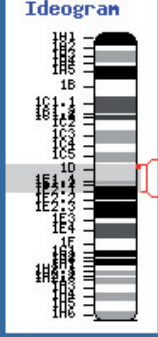
57.98

70.34

[Go](#)

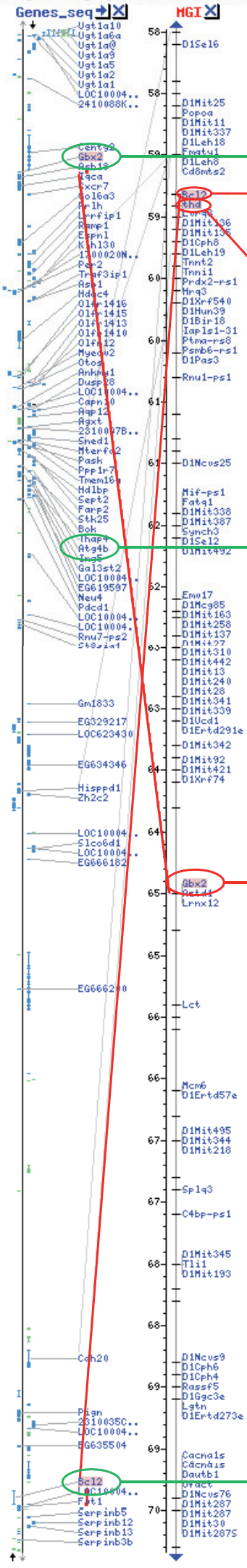
out
 zoom
 in

You are here:



default
 master

Region Displayed: 57.98-70.34 cM



Gbx2

Bcl2

Thd

Atg4B

Gbx2

Bcl2

SUPPLEMENTARY FIGURE LEGENDS

Supplemental Figure 1. Analysis of proteasome-mediated protein degradation in *Atg4B*^{-/-} MEFs. Murine Embryonic Fibroblasts (MEFs) were metabolically labelled and chased as described in Materials and Methods, in the absence or presence of proteasome inhibitor lactacystin. To allow optimal inhibition and to avoid secondary effects, protein degradation was measured at different time points starting after 1 h and continuing for an additional 3 h period. The contribution of proteasome to total protein degradation was calculated as described in Material and Methods (percentage of the labelled protein whose degradation was inhibited per hour). Results are the mean and standard deviation from 4 separate experiments with duplicate samples. Four *Atg4B*^{+/+} and three *Atg4B*^{-/-} independent cell lines were used.

Supplemental Figure 2. Analysis of starvation-dependent degradation of p62, pro-LC3 electrophoretic mobility and lipidation of Atg8-like proteins in WT and *Atg4B*^{-/-} mouse tissues. (A) Representative immunoblots of endogenous p62 in tissue extracts from age-matched control and mutant mice subjected to the indicated starvation conditions or fed *ad libitum*. Protein extracts from two mice per genotype and condition are shown. β -actin was used as loading control in all tissues except in heart (α -tubulin). (B) Representative immunoblots of murine LC3 from WT and *Atg4B*^{-/-} MEFs showing the electrophoretic mobility of LC3-I, LC3-II and recombinant pro-LC3 produced in *E. coli*. C- stands for an *E. coli* lysate not expressing LC3 cDNA (C) Representative immunoblots of endogenous LC3 in tissue extracts from age-matched control and mutant mice subjected to the indicated starvation conditions or fed *ad libitum*. Protein extracts from two mice per genotype and condition are shown. Note that only liver and skeletal muscle from mutant mice present a clear LC3 lipidation after starvation, whereas most of WT derived tissues present LC3 lipidation. β -actin was used as loading control in all tissues except in heart and skeletal muscle (α -tubulin). (D) Representative immunoblots of endogenous LC3 in tissue extracts from age-matched control and mutant mice subjected to the indicated starvation conditions or fed *ad libitum*. Protein extracts from two mice per genotype and condition are shown. Note that GABARAP protein levels decrease after starvation in a tissue-dependent fashion both in WT and mutant samples, but levels in *Atg4B*^{-/-} are always lower. β -actin was used as loading control in all tissues except in heart and skeletal muscle (α -tubulin). (E) Representative

immunoblots of endogenous LC3 in tissue extracts from age-matched control and mutant mice subjected to the indicated starvation conditions or fed *ad libitum*. Protein extracts from two mice per genotype and condition are shown. As for GABARAP, ATG8L protein levels decrease after starvation in a tissue-dependent fashion both in WT and mutant samples, but ATG8L protein levels are always lower in *Atg4B*^{-/-} samples.

Supplemental Figure 3. Histological analyses of CNS from affected *Atg4B*-null mice.

H&E staining and anti-ubiquitin immunohistochemistry in different CNS sections from WT (up), affected *Atg4B*^{-/-} (middle) and nestin-Cre/*Atg7*^{lox/lox} mice (down), which were used as a positive control. **(A)** H&E in cerebellar sections at 10X (left) and 40X (middle) magnification showing that affected *Atg4B*^{-/-} mice maintain the histological characteristics of this part of CNS including Purkinje cell layer, practically absent in nestin-Cre/*Atg7*^{lox/lox} mice (arrowhead in middle-bottom panel). Right panels show that the characteristic massive accumulation of ubiquitylated-protein aggregates present in nestin-Cre/*Atg7*^{lox/lox} mice (arrow) is not observed in WT samples or in those from affected *Atg4B*^{-/-} mice. **(B)** H&E in vestibular nuclei sections at 10X (left) and 40X (middle) magnification. *Atg4B*^{-/-} mice do not show axonal degeneration, manifested by the presence of eosinophilic spheroids characteristic of nestin-Cre/*Atg7*^{lox/lox} mice (arrowheads in middle-bottom panel and inset). Affected *Atg4B*^{-/-} mice do not present accumulation of ubiquitylated-protein aggregates in neuronal cells (right panels). In contrast, nestin-Cre/*Atg7*^{lox/lox} mice present accumulation of ubiquitylated proteins in neurons from vestibular nuclei (arrows and inset in bottom-left panel). **(C)** H&E in hippocampus sections at 10X (left) and 40X (middle) magnification. No histological alterations were observed in any of the models analyzed in this CNS section. Nestin-Cre/*Atg7*^{lox/lox} mice accumulate poly-Ub aggregates (inset in bottom-right panel), whereas they are not observed in WT or affected *Atg4B*^{-/-} mice. **(D)** Cerebral cortex H&E sections at 10X (left) and 40X (middle) magnification. No histological alterations were observed in any of the models analyzed in this CNS section, with the exception of occasional axonal swelling in nestin-Cre/*Atg7*^{lox/lox} samples (data not shown). Nestin-Cre/*Atg7*^{lox/lox} mice present accumulation of ubiquitylated proteins in neurons, whereas these aggregates were not observed in WT or affected *Atg4B*^{-/-} samples. *Note that anti-Ub antibody reacts with cellular nuclei in a non-specific manner. **(E)** TUNEL assay in cerebellar sections showing the characteristic massive apoptosis of autophagy-ablated nestin-Cre/*Atg7*^{lox/lox} mice (bottom) but not in WT (up) or affected *Atg4B*^{-/-} mice (middle).

Supplemental Figure 4. Autophagy-impaired mice present an accumulation of abnormal globular substance in utricular/sacculus lumen. (A) Representative semithin sections of WT and *Atg4B*^{-/-} mice utricles (left panels) showing the presence of otoconial crystals (arrows) and nascent globular substances (arrowheads) in WT samples. In contrast, *Atg4B*^{-/-} samples exhibited an accumulation of globular substances that usually presented a less dense content than those from WT mice as well as one or several internal vesicles (middle and left panels). (B) H&E sections from neonate mice utricles (left panels) showing the presence of normal otoconial crystals in WT samples (arrows) and an accumulation of eosinophilic globular substances in *Atg5*^{-/-} neonates (arrowheads). At the ultrastructural level (right panels), *Atg5*^{-/-} globular substances presented similar features than those observed in *Atg4B*^{-/-} mice. Scale bars: 15 μm in semithin and H&E sections; 1 μm in TEM panels.

Supplemental Figure 5. Streptomycin treatment induces cell vacuolization associated with autophagy impairment in cultured MEFs. MEFs were cultured in conventional fibroblasts medium supplemented with 1mg/mL of streptomycin sulfate. As seen in (A), p62 accumulation is clearly detected after 6 days of incubation. This phenomenon is accompanied by massive vacuolization (B). Higher doses of streptomycin resulted in an increase of cell-death associated with precocious massive cell vacuolization.

Supplemental Figure 6. Relative position of tilted-head (*thd*) allele and *Atg4B* genomic locus. Physical genomic map (left), showing the location of *Atg4B* on murine chromosome 1. *Bcl2* and *Gbx2* loci are depicted as references and are stressed in green in their physical position on chromosome 1. MGI genetic map (right) shows the relative position of *thd* allele in the same genomic region that *Atg4B* locus. *Bcl2* and *Gbx2* loci are also used as a reference and are stressed in red in their genetic location (shown in cM). Note that *Bcl2* and *Gbx2* loci are inverted in the genetic map as compared to their physical location. Image modified from NCBI map viewer (<http://www.ncbi.nlm.nih.gov/mapview/>)